

Study of the suitability of silica based xerogels synthesized using ethyltrimethoxysilane and/or methyltrimethoxysilane precursors for aerospace applications

Marta Ochoa · Luísa Durães · Ana Matos Beja · António Portugal

Received: 4 May 2011 / Accepted: 3 October 2011 / Published online: 12 October 2011
© Springer Science+Business Media, LLC 2011

Abstract Silica based materials were synthesized using ethyltrimethoxysilane (ETMS) and/or methyltrimethoxysilane (MTMS) precursors by sol–gel technology, in order to ascertain if their properties are suitable for aerospace applications. When ETMS was used alone and in equimolar ETMS/MTMS mixtures, no gel formation took place and a resin-like precipitate was observed. After drying, a compact tablet was formed. When mixtures of 25% ETMS/75% MTMS and MTMS alone were used, gel formation occurred and xerogels were produced upon drying. Chemical and structural characterization of the obtained materials was performed using Elemental Analysis, FTIR, XRD and SEM. Bulk density, specific surface area, contact angle and the thermal behavior were also evaluated. For materials from ETMS, the chemical structure grows preferentially in one direction and, in the case of MTMS the growth follows a 3D pattern. The use of ETMS precursor leads to a significant increase in the product density, accompanied by a decrease in the specific surface area. It also leads to a decrease in the thermal stability limit of the synthesized materials. Then, ETMS precursor is less appropriate than MTMS precursor for space applications. However, ETMS co-precursor in mixtures with MTMS contributes to the increase in the hydrophobic character of the synthesized materials.

Keywords Amorphous materials · Sol–gel chemistry · Microstructure · Hydrophobicity · Aerospace

1 Introduction

Silica based materials synthesized by sol–gel technology have exceptional properties, namely very low density, high specific surface area, low thermal conductivity and high transparency allowing their use in several applications, as thermal or acoustic insulators, dielectric or optical materials, catalysts and sensors [1, 2]. When lightweight, porous, flexible and hydrophobic they are particularly suitable for aerospace applications, mainly as thermal and structural insulators for re-entry and Mars vehicles, spacecraft components, spacesuits, cryogenic tanks, space station buildings, *etc.* The requirements for space application are: density, from 10 to 100 kg/m³; thermal conductivity, from 3 to 16 mW/(m K); working pressure, from 10 to 10³ Pa; working temperature, from –150 to 500 °C; moderate flexibility [3–5]. In previous works, with MTMS precursor, materials that had density in the range 40–100 kg/m³, specific surface area of ~400 m²/g, high hydrophobicity (>130°) and moderate flexibility were obtained [3–8], and these properties make them excellent candidates for aerospace applications. Thus, the use of the ETMS precursor was studied for the same applications, since with this precursor the group that remains in the 3D solid network (ethyl) is larger than with MTMS precursor (methyl)—Fig. 1—and, by this reason, it was expected that it would increase the porosity and hydrophobicity. Some authors [9, 10] referred that, when ETMS alone was used the gelation did not occur. However, when used as co-precursor in mixtures with tetraethylortosilicate (TEOS) and tetramethylortosilicate (TMOS), gels are obtained and the final

M. Ochoa · L. Durães (✉) · A. Portugal
CIEPQPF, Department of Chemical Engineering, University of Coimbra, Pólo II, Rua Sílvio Lima, 3030-790 Coimbra, Portugal
e-mail: luisa@eq.uc.pt

A. M. Beja
CEMDRX, Department of Physics, University of Coimbra, Rua Larga, 3004-516 Coimbra, Portugal

materials exhibit low density ($<70 \text{ kg/m}^3$), low thermal conductivity ($\sim 3 \text{ mW/(m K)}$) high contact angle ($>140^\circ$) [9–14]. But, although these precursors are cheaper than trialkoxysilanes and some of their product properties appropriate for space applications, the obtained materials are rigid and brittle, thus they cannot absorb vibration in space conditions without fragmentation [3].

In this work, the viability of gel formation using the ETMS precursor alone or in mixtures involving MTMS is studied. A comparison of the physical, chemical and structural properties of all the synthesized materials was made, taking for reference the material synthesized only with MTMS. Additionally, their thermal behavior/stability up to $1,000^\circ \text{C}$ was investigated. The suitability of all obtained materials for application in aerospace industry was also evaluated.

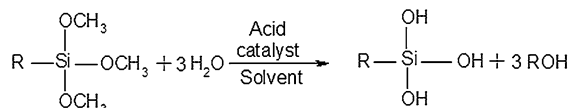
2 Materials and Methods

The overall experimental procedure in this study followed the methods described earlier [3–8] for MTMS precursor.

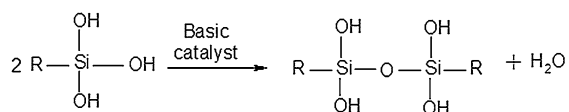
2.1 Synthesis

MTMS ($\text{CH}_3\text{Si}(\text{OCH}_3)_3$, 98%, Aldrich), ETMS ($\text{C}_2\text{H}_5\text{Si}(\text{OCH}_3)_3$, 97%, Aldrich), methanol (CH_3OH , 99.8%,

Hydrolysis reaction:



Condensation reaction:



Polycondensation reaction:

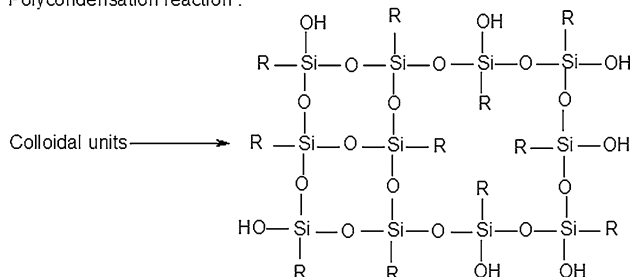


Fig. 1 Sol-gel reaction mechanism for trialkoxysilanes (R = CH_3 or CH_2CH_3 , for MTMS or ETMS, respectively)

Riedel-de Haën), oxalic acid ($\text{C}_2\text{H}_2\text{O}_4$, 99%, Fluka) and ammonium hydroxide (NH_4OH , 25% in water, Fluka) were used as precursors, solvent, acid and basic catalysts, respectively. Before the synthesis, acid and basic catalyst solutions were prepared: 0.1 M oxalic acid solution and 13.2 and 10 M ammonium hydroxide solutions.

In the first step of the synthesis, the precursor is mixed with methanol and the oxalic acid solution. The water of the oxalic acid solution promotes the hydrolysis. In the second step, 24 h later, the ammonium hydroxide solution is slowly added. The condensation of monomers $\text{RSi}(\text{OH})_3$ become significant, forming a sol.

During the first two steps, the temperature is controlled at 25°C by means of a glass jacket with flowing water from a thermostatic bath.

In this study, samples were prepared from pure ETMS and MTMS precursors and their mixtures in different proportions (Table 1). Defining S, A and B as the molar ratios, methanol/precursor, acidic water/precursor and basic water/precursor, respectively, the used values for these ratios were $S = [35, 20, 10]$, $A = 4$ and $B = 4$. For sample I, we tested 10 and 13.2 M ammonium hydroxide solutions, whereas for all the other samples a 10 M ammonium hydroxide solution was used.

The prepared solutions were then placed in an oven at 27°C where gelation occurs.

Finally, the gels were aged for 2 days at 27°C and dried at ambient pressure to produce the xerogels. The temperature cycles used in the drying stage were: 24 h at 60°C , followed by three stages, at 100, 150 and 200°C , of 1 h each.

2.2 Characterization

Several techniques were used for the chemical, physical and thermal characterization of the xerogels. Elemental analysis was performed using *Fisons Instruments* model EA 1108 CHNS-O apparatus. Structural characterization was done by FTIR (*Nicolet 6700, Thermo Scientific*) and Transmission XRD in a 0.5 mm capillary (*Enraf-Nonius FR 590 diffractometer*). The XRD equipment was composed by a Cu radiation source (Long Fine Focus), a quartz monochromator and an *Inel CPS 120* detector. Thin pressed pellets (80 mg of KBr and 0.6 mg of xerogel) were used for FTIR analysis. The microstructure of the xerogels was observed by SEM (*JOEL JMS-5310*), using 15 or 20 kV voltages for the electron beam acceleration. The xerogels were previously coated with a gold film to increase their conductivity. The bulk density of the xerogels was determined directly by the ratio mass/volume, weighting and measuring the dimensions of regular sample pieces. The nitrogen gas adsorption/desorption isotherms of xerogels were measured using a *Micromeritics*

Table 1 Samples identification and masses of the dried materials

Sample type	Molar percentage of precursor(s)	Product form	Product mass per synthesis (g)
I	100% ETMS	Compact tablet	2.477
II	50% MTMS and 50% ETMS	Compact tablet	2.264
III	75% MTMS and 25% ETMS	Xerogel	2.426
IV	100% MTMS	Xerogel	2.231

ASAP2000 analyzer. The BET specific surface areas were estimated by the Brunauer–Emmett–Teller method and the average pore diameters were obtained by the Barrett–Johner–Halendar (BJH) method. The pore size distributions were calculated from the analysis of desorption isotherms for the pore size range 1.7–300 nm. The contact angle of water in the xerogels was measured by a *Contact Angle System OCA 20*, from *Dataphysics*. The thermal behavior/stability of the xerogels was evaluated by DSC-TG simultaneous thermal analysis, using a heat flux DSC *SDT Q600*, from *TA Instruments*. A heating rate of $10\text{ }^{\circ}\text{C min}^{-1}$ and a nitrogen atmosphere were used in all the tests.

3 Results and discussion

For samples I and II, prepared from the ETMS precursor alone and from 50/50 precursors mixture, no gel formation took place for at least 8 days. In this case, the resulting precipitates/resins led to compact tablets after drying. Gels were successfully obtained from samples III (75% MTMS and 25% ETMS) and IV (MTMS) after ~ 2 days and ~ 5 h, respectively. In the sol solution obtained with ETMS precursor, the length and weight of the substituent group promotes the phase separation of the hydrolyzed species from the less dense alcoholic phase [10]. Thus, the condensation does not occur in the overall solution volume due to the sedimentation of monomers in the bottom of the container. The higher concentration of the monomer in the bottom leads to localized polycondensation and formation of a resin-like phase that originates the compact tablets after drying. This effect is not so significant when the ETMS precursor is used in mixtures with a major amount of the MTMS precursor, as faster gelation occurs in these cases. It is worth to mention that only a maximum waiting period of 8 days was considered for the samples I and II, since longer times would be prohibitive for industrial applications and, furthermore, the phase separation was soon observed in the first days of this period.

The mass of the dried materials (xerogels and tablets) per synthesis are shown in Table 1. The values are analogous in all the four samples, proving that the amount of the condensed material is equivalent in all cases, even in cases where there was no gel formation.

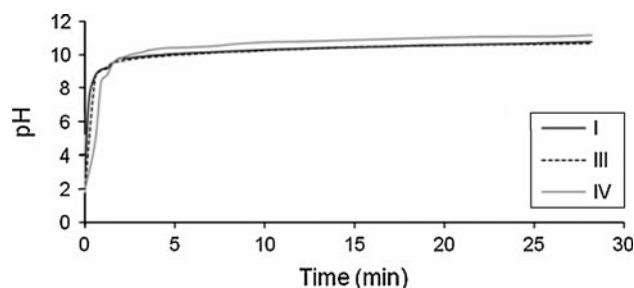


Fig. 2 pH evolution during the basic catalysis step. Examples for samples I, III and IV

The pH was measured during the addition of the basic solution (Fig. 2) and its evolution was similar for all samples. Starting from a pH ~ 2 (hydrolysis stage), a sharp pH increase up to ~ 9 was observed with the addition of the first 2–3 drops of the basic catalyst solution. After that, the solution became cloudy and milky, a clear indication of the onset of the colloidal particles formation. With further addition of basic catalyst solution, the pH increased slowly and leveled off at a value of ~ 11 .

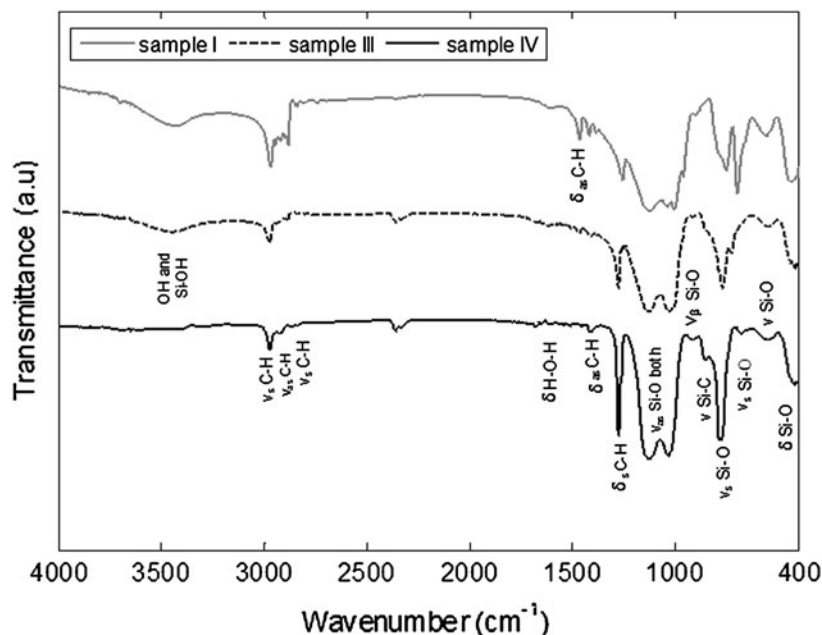
Therefore, with the previous results it may be concluded that the condensation reaction took place in an extensive way in all materials, but the organization of the three-dimensional network was not similar.

The expected structure of the inorganic polymer can be estimated considering complete condensation (condensation of all hydroxyl groups). In this case, the estimated elemental molar ratios, for materials obtained from samples I, II, III and IV, are respectively 1Si:1.5O:2C:5H, 1Si:1.5O:1.5C:4H, 1Si:1.5O:1.25C:3.5H and 1Si:1.5O:1C:3H, neglecting the contribution of the OH terminal groups of the network ends. The corresponding estimated mass ratios and the obtained elemental analysis results are shown in Table 2.

The values of wt% C will be used to assess the extension of the condensation reaction, since the amount of the other elements is significantly affected by other factors. The amount of nitrogen, although small, confirms the presence of residues of the basic catalyst in the dried material. These residues also contain H and O. The elemental analysis furnace operates at 1,333 K for the O determination, which is not an enough high temperature to break the Si–O bonds. This justifies the very low experimental values obtained for

Table 2 Calculated and experimental mass percentages of C, H, O and N elements for the synthesized materials

Sample	wt% C		wt% H		wt% O		wt% N
	Calc.	Exp.	Calc.	Exp.	Calc.	Exp.	
I	29.6	28.8	6.21	7.30	26.9	0.74	0.30
II	24.3	23.9	5.44	6.55	29.2	0.66	0.39
III	21.3	21.8	4.99	6.08	30.5	0.63	0.27
IV	17.9	17.8	4.51	5.41	35.8	0.69	0.11

Fig. 3 FTIR results for the produced materials based on samples I (ETMS), III (25% ETMS/75% MTMS) and IV (MTMS)

the oxygen element (see Table 2). Comparing the estimated and experimental mass percentages of carbon, the results show that the condensation can be considered complete in samples III and IV. For samples I and II, the experimental values of the wt% C are slightly lower than the calculated values. Thus, in these cases the condensation appears to be not so extensive, especially in sample I, i.e. part of the OH groups didn't suffered condensation and remained in the structure. Notice that the estimated wt% C for incomplete condensation is lower than for complete condensation due to the higher amount of the oxygen per Si atom.

The typical FTIR spectra of the synthesized materials—Fig. 3, show several bands corresponding to the various structural units of the solid network. A complete list of the vibration frequencies and their assignments are compiled in the Appendix. The broad band observed for samples I and III at $\sim 3,500\text{ cm}^{-1}$ corresponds to the overlapping of the O–H stretching vibrations of hydrogen-bonded to water molecules and SiO–H stretching vibrations of the silanols hydrogen-bonded to water molecules. The band at 960 cm^{-1} , ascribed to the Si–O stretching vibrations of the

silanol Si–OH groups, is also observed for the same samples (I and III). These bands do not appear in sample IV, revealing that the condensation was more extensive for the sample synthesized with MTMS alone. Near $1,650\text{ cm}^{-1}$ appear the bands corresponding to the deformation vibration of H–O–H bonds. The intense bands at $\sim 760\text{ cm}^{-1}$ and between $1,000$ and $1,150\text{ cm}^{-1}$ are due to symmetric and antisymmetric stretching vibrations of Si–O bonds, respectively. These are more intense for sample IV, confirming the conclusion about the completeness of the condensation reaction in this xerogel. The symmetric and antisymmetric deformation vibrations of C–H bonds appear between $\sim 1,200\text{ cm}^{-1}$ and $\sim 1,500\text{ cm}^{-1}$ and the symmetric and antisymmetric stretching vibrations of the same bonds are found between $\sim 2,800\text{ cm}^{-1}$ and $3,000\text{ cm}^{-1}$. The structural units detected in the xerogels, through the characteristics vibration frequencies, confirmed the hypothetical structure of an inorganic network based on Si–O bonds, with a methyl or ethyl group per Si and –OH terminal groups at the network ends. It is clear that the type of vibrations related to the ethyl structural unit were more noticeable in sample I (ETMS), as expected. Furthermore,

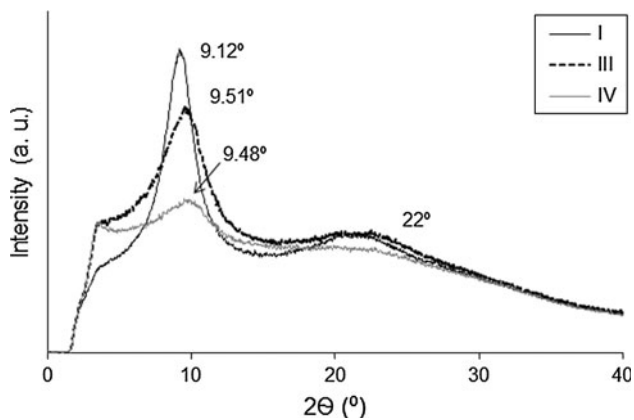


Fig. 4 XRD patterns for the produced materials based on samples I (ETMS), III (25% ETMS/75% MTMS) and IV (MTMS)

the vibrations attributed to the Si–OH groups were more intense in the same sample, in agreement with the elemental analysis conclusions.

Figure 4 shows the XRD patterns of the synthesized materials. The obtained diffraction patterns are characteristic of materials with very low crystallinity. Two broad diffraction peaks can be distinguished, centered approximately at 9° and 22° (2θ), in agreement with the XRD results obtained by other authors for similar materials [15, 16]. The first peak may be related to the spacing between silicon atoms attached to the alkyl group (methyl or ethyl) and is indicative of channels of alkyl groups in the structure [15]. Thus, this peak is absent for silica structures without the organic group. From Fig. 4 it can be observed that the

intensity of this peak increases with the length of the alkyl group, indicating that the channels produced by the ethyl group in the material structure are more pronounced when compared to the case of the methyl group, as expected. The second peak, at ~22°, is associated with the spacing of Si atoms and angle of the group Si–O–Si, and, as compared by Lana et al. [15], crystalline silica materials have a sharper peak than amorphous silica materials (including those obtained by sol–gel processing). In the present work results, this peak is very broad and diffuse for all the samples, especially in the case of sample IV. Nevertheless, the peak is slightly more intense when ETMS was used in the precursor system. This might be due to the fact that ETMS precursor contributes for some crystalline order (but low) in the structure of the xerogels.

Figure 5 shows SEM images of the compact tablet obtained with 100% ETMS. On the material’s surface, large rectangular holes and some spherical particles can be observed (Fig. 5a). These spherical particles are connected to the matrix, but they had no conditions or time to integrate the matrix material. In Fig. 5b, which corresponds to the material interior, some circular pores are visible. They may be due to gas retention within the structure. Fig. 5c shows small clusters of condensed particles that remained inside the pores. The structure of these clusters appears to be an early stage of condensation, before the spheres formation. Thus, the condensed structure seems to grow preferentially in one direction when the alkyl group is larger (see Fig. 5d). These micro-clusters should have been formed initially in the whole sample, but they end up

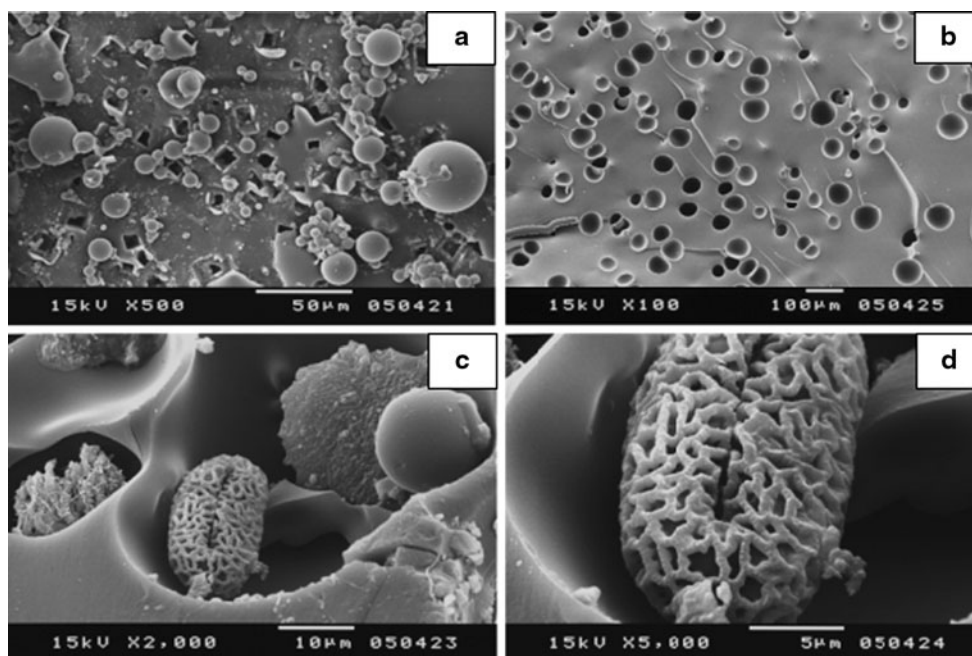


Fig. 5 SEM images of materials prepared from sample I (ETMS): **a** surface, **b–d** interior (material previously cut)

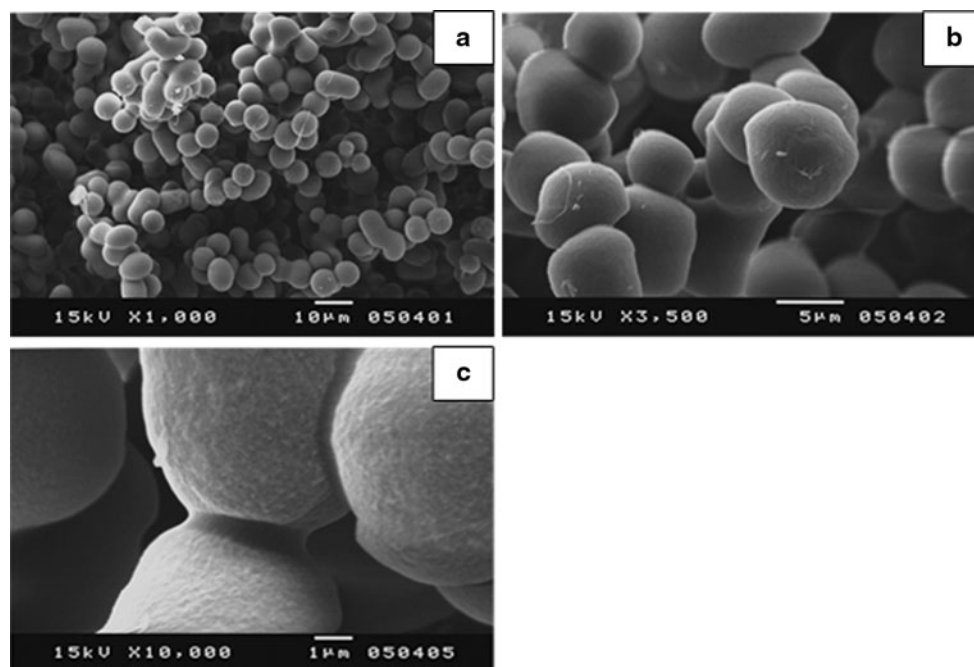


Fig. 6 SEM images of xerogels synthesized with 75% MTMS/25% ETMS mixture (sample III)

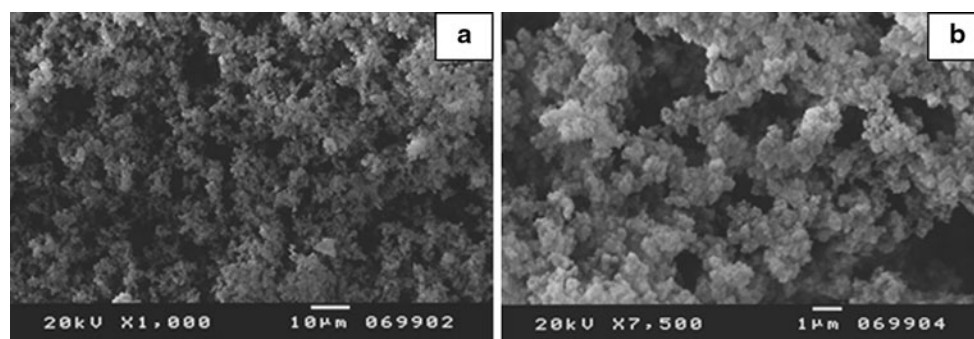


Fig. 7 SEM images of xerogels obtained from sample IV (MTMS)

together and filled by additional condensation reactions, resulting in a compact solid.

Figure 6 shows images of silica based xerogels synthesized from 75% MTMS/25% ETMS mixture (sample III). In Fig. 6a,b, clusters of approximately spherical structures with diameter of 5–10 μm can be observed. In Fig. 6c, the necks that connect the structural units are visible. Whole material presents this microstructure, resulting from the connection between the spherical units (3D solid skeleton).

Images of the material synthesized with 100% MTMS (sample IV) are presented in Fig. 7a,b. The xerogel structure clearly grew in three dimensions and was formed from a binding mechanism of very small spherical units (much smaller than 1 μm).

Comparing the SEM images obtained for xerogels prepared with 100% MTMS (sample IV) and 75% MTMS

(sample III)—Figs. 6 and 7, a significant increase of the condensed units in sample III is apparent, which is due to a ETMS contribution of only 25% in the precursor system. The ethyl group is larger than the methyl what contributes to the increase of steric hindrance in the medium and the consequent decrease of the condensation rate, giving rise to more linear (less ramified) structures. This effect, overlapped with some sedimentation of the monomers, dimers, trimers, etc., due to its higher weight (increasing its local concentration), enhances the increase of the condensed units. Thus, the ETMS influences significantly the organization of the solid network, resulting in the observed modifications of the xerogels structure.

Table 3 presents the density ranges of the synthesized materials. The ETMS precursor contributes to a significant increase in the density of the synthesized materials. This was expected considering the microstructures observed by

Table 3 Density ranges obtained for the synthesized materials

Sample	Density range (kg/m ³)
I	[794, 1,089]
II	[469, 870]
III	[104, 234]
IV	[89, 125]

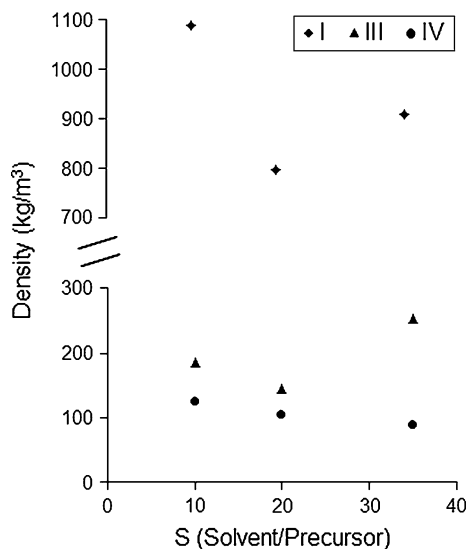


Fig. 8 Influence of the precursor dilution on the densities of materials obtained from samples I (ETMS), III (25% ETMS) and IV (MTMS)

SEM and the already discussed mechanisms of the materials formation/growth.

The density of the obtained materials as a function of the S molar ratio is shown in Fig. 8.

The effect of the S molar ratio on the density was studied by Durães et al. [3] for the case of 100% MTMS. They concluded that a higher S resulted in lower density of the xerogels, which is due to a higher dilution of the precursor and, thus, less extension of the cross-linking. This is confirmed in the present work for sample IV. However, for materials obtained with ETMS (sample I) and with 25% ETMS (sample III) the lowest density was achieved for S = 20. In these cases, the dilution effect predominates only up to S = 20. Above this value, the decrease in the condensation rate is significant and the sedimentation of monomers is more pronounced, leading to a densification of the final material. This effect was observable by the higher amount of liquid remaining above the solid phase for S = 35.

Figure 9 shows the nitrogen gas adsorption/desorption isotherms obtained for samples I, III and IV. In the cases of the xerogels obtained with 100% MTMS (sample IV) and 75% MTMS (sample III), the isotherms have a profile

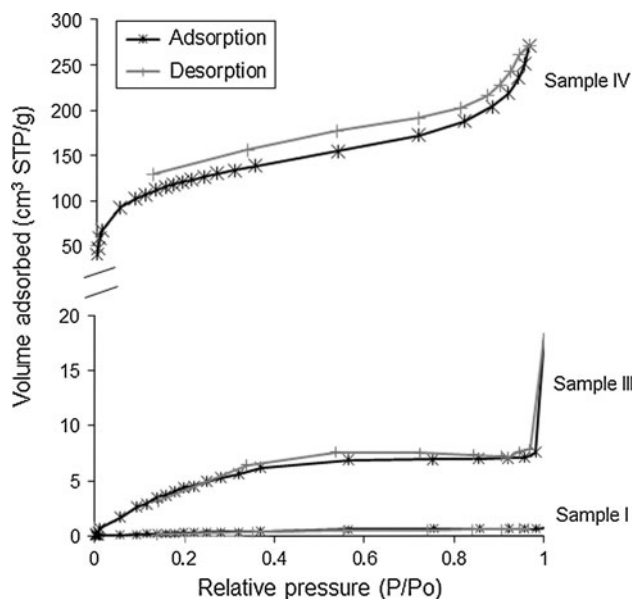


Fig. 9 Nitrogen gas adsorption/desorption isotherms obtained for samples I, III and IV

Table 4 Specific surface area, pore size and contact angle of the synthesized materials

Sample	S	BET specific surface area (m ² /g)	BJH average pore size (Å)	Contact angle (°)
I	20	1.68 ± 0.07	43	126 ± 4
	35	1.47 ± 0.04	42	–
III	20	2.94 ± 0.25	45	140 ± 4
	35	5.49 ± 0.17	50	–
IV	20	21.23 ± 1.06	20	142 ± 5
	20	416.39 ± 8.66	42	129 ± 2

similar to type IV isotherms, although, with sample IV, the adsorbed N₂ volume is significantly higher than is for sample III. This type of isotherm is characteristic of mesoporous materials. For the dense material obtained with 100% ETMS (sample I), the obtained isotherm shows a profile between type II and I isotherms, thus the hysteresis loop is absent. Type II isotherms are typical of nonporous materials, fact that is agreement with the very low amount of N₂ adsorbed by sample I. Type I isotherms are observed in microporous materials that adsorb mainly at low relative pressures. Possibly the few existing pores in sample I are micropores, justifying the obtained intermediate profile of the adsorption isotherm.

Table 4 shows the results from ASAP2000 analyses. It is clear that the specific surface area increases with the MTMS proportion in the precursor system, which agrees with the observed decrease in density and the isotherms profiles. Comparing the results of the xerogel obtained with

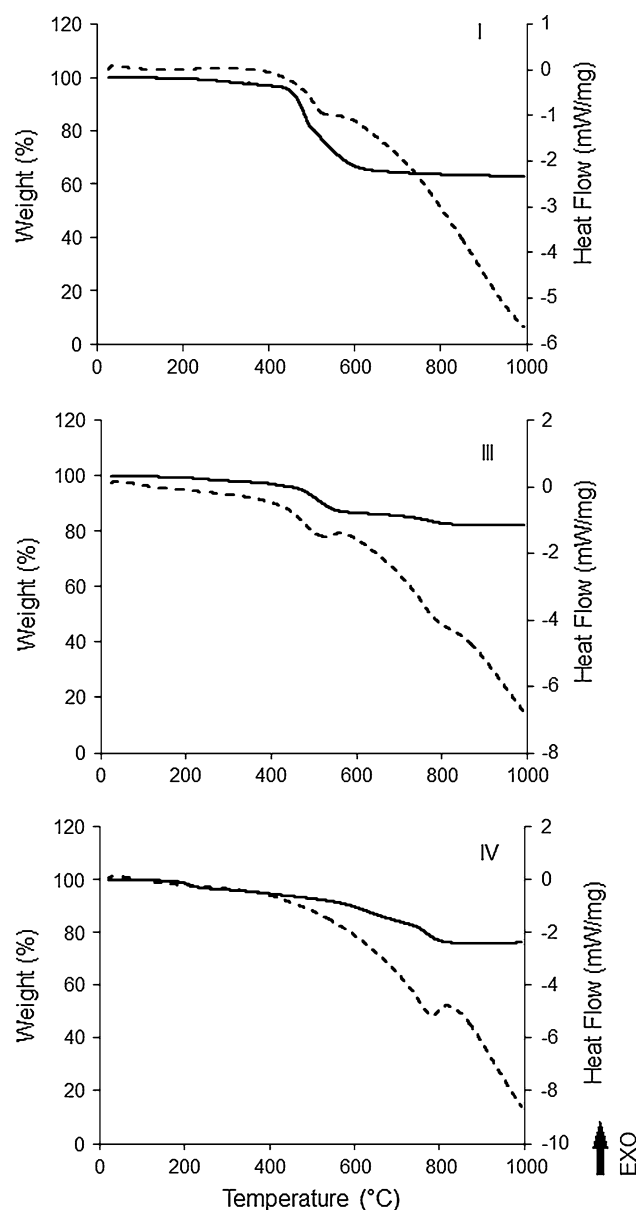


Fig. 10 DSC-TG curves for the produced materials based on samples I (ETMS), III (25% ETMS/75% MTMS) and IV (MTMS): *solid lines* Weight; *dotted lines* Heat flux

75% MTMS and the xerogel obtained with 100% MTMS (last two rows of the table), there is a considerable difference in specific surface area values. This difference was expected, considering the results obtained by SEM, since the ETMS precursor contributed for a substantial increase in the spherical structural units of the xerogels. The magnitude of the average pore diameter leads to the conclusion that the obtained materials are mainly mesoporous. However, the pore diameters evaluated by this technique have only indicative value, justifying the different conclusions obtained for sample I by analyzing the profile of the isotherms and the average pore diameter.

The obtained contact angle values were higher than 120° (Table 4), proving the high hydrophobic character of the synthesized materials. This is due to the presence of the ethyl and methyl groups in their chemical structure. Sample I had more hydroxyl groups in the structure and, accordingly, it exhibits the lower contact angle value. The longer aliphatic group (ethyl) may possibly cause an increase in the contact angle, but in sample I this effect was over shaded by the contrary effect of the OH groups. As the significance of the OH groups decreases with the amount of ETMS in the precursor system, this cancellation may have not occurred in samples II and III, which have higher contact angle values. Thus, it seems that the ETMS coprecursor in mixtures with MTMS may contribute to the increase of the xerogels hydrophobicity, opening the way to applications where this is a critical property.

Finally, the DSC-TG curves are presented in Fig. 10 and the corresponding weight losses and temperatures for the observed thermal phenomena are indicated in Table 5. It should be mentioned that the falling of the DSC baseline is inherent to the used equipment. As can be observed, all samples lose a small part of its weight in lower temperatures (up to $\sim 400^\circ\text{C}$), but this loss increases with the amount of MTMS in the precursor system. This can be explained by the slow and progressive evaporation of the retained solvent, catalysts and other impurities, which are entrapped in the xerogels/tablets structure. In fact, the major part of this loss happens after 200°C , that is the end temperature of the drying cycles. More, with the increasing amount of MTMS in the precursor system, the porosity and surface area of the synthesized materials increase significantly, especially from sample III to sample IV, favoring the adsorption phenomenon of these compounds. In this temperature range, also some terminal hydroxyl groups may leave the silica structure. The mentioned phenomena are usually endothermic, however as they occur very gradually they are not perceptible in the DSC curves.

Further weight losses, and more significant, occur at temperatures higher than $\sim 400^\circ\text{C}$ (Fig. 10 and Table 5) and these are accompanied by endothermic peaks in the DSC curve. These can be justified by the thermal decomposition, in a non-oxidizing atmosphere, of the methyl and ethyl groups attached to silicon, what happens in two stages (observe also the different slopes in the weight drop in sample I). The weight loss after 400°C is much larger in sample I than in the other two samples, which can be explained by the higher weight of the ethyl group when compared to the methyl group. If complete hydrolysis and condensation reactions are considered, the weight percentages of the methyl and/or ethyl expected in the final materials would be 35.8, 26.3 and 22.4 wt% (C + H)—see Table 2—for samples I, III and IV, respectively. Comparing these values with the sum of weight losses after $\sim 400^\circ\text{C}$, it

Table 5 Weight losses and temperatures of the thermal phenomena identified in the DSC-TG analyses of the synthesized materials

Sample	TG		DSC		
	T _{ini} -T _{end} (°C)	Weight loss (%)	Type of peak	T _{onset} (°C)	T _{peak} (°C)
I	24–374	2.7	NP	–	–
	374–993	34.3	Endothermic	552	596
III	24–436	3.7	NP	–	–
	436–636	9.9	Endothermic	438	517
	636–993	4.1	Endothermic	731	792
IV	22–439	5.9	NP	–	–
	439–715	10.2	NP	–	–
	715–993	7.6	Endothermic	727	779

NP Not perceptible

Table 6 Characteristic vibration frequencies (cm⁻¹) of FTIR spectra of the synthesized materials

Sample I	Sample III	Sample IV	Type of vibration [13]	Structural unit [13]
438	418	418	δ O–Si–O	O–Si–O
563	550	550	ν Si–O	SiO ₂ defects
695	728	682	ν_s Si–O	\equiv Si–O–Si \equiv
752	770	781	ν_s Si–O	\equiv Si–O–Si \equiv
–	–	854	ν Si–C	Si–R
921	920	921	ν_β Si–O	Free Si–O ⁻
960	960	–	ν_β Si–O	\equiv Si–OH
1,007	1,030	1,032	ν_{as} Si–O	\equiv Si–O–Si \equiv
1,127	1,128	1,127	ν_{as} Si–O	\equiv Si–O–Si \equiv
1,256	1,274	1,273	δ_s C–H	Si–R
1,384	1,384	–	δ_s C–H	–CH ₂
1,417	1,417	1,407	δ_{as} C–H	Si–R
1,467	1,467	–	δ_s C–H δ_{as} C–H	–CH ₂ –CH ₃
1,653	1,650	1,683	δ H–O–H	H–O–H
2,842	2,843	2,842	ν_s C–H	–CH ₂
2,883	2,862	2,862	ν_{as} C–H	–CH ₃
2,923	–	–	ν_{as} C–H	–CH ₂
2,943	–	–	ν_{as} C–H	–CH ₂
2,967	2,973	2,971	ν_s C–H	–CH ₃
3,445	3,461	–	O–H and SiO–H	H–O–H...H ₂ O and \equiv SiO–H...H ₂ O

ν stretching vibration, ν_s symmetric stretching vibration, ν_{as} anti-symmetric stretching vibration, ν_β in-plane stretching vibration, δ deformation vibration, δ_s symmetric deformation vibration (bending), δ_{as} antisymmetric deformation vibration (bending)

can be concluded that they agree well but the thermal decomposition of alkyl groups in sample III was not so extensive. In addition, it should be noted that the referred decompositions are observed in increasing temperatures when the amount of MTMS in the precursor system

increases, showing that the use of the MTMS precursor leads to materials with a higher thermal stability limit and thus more appropriate for Space applications. The first significant weight losses observed in samples III and IV begins at ~440 °C, which is very close to the end of the working temperature interval for Space applications (500 °C).

4 Conclusions

Silica based materials were synthesized by sol–gel technology from precursors MTMS and ETMS alone or in combination. In the case of ETMS precursor alone and of the mixture with 50% of each precursor, compact tablets were obtained. When mixtures of 75% MTMS/25% ETMS and MTMS precursor alone were used, xerogels were produced.

The characterization of the materials show that, when the alkyl derivative group is larger (as in ETMS), growth of structure in a preferential direction seems to occur, resulting in a more linear structure. On the contrary, when MTMS is used, a branched structure is obtained.

The introduction of ETMS as a co-precursor in mixtures with MTMS contributes to an increase in density and in the size of the structural units. Consequently, a decrease in the specific surface area and porosity is observed. In addition, it contributes to a decrease in the thermal stability limit of the synthesized materials. Thus, it can be concluded that the use of this precursor, to synthesize xerogels for application in the aerospace industry, is less favorable than the use of the MTMS precursor alone. Still, ETMS seems to contribute to an increase in the contact angle values of the final materials, thus being a suitable co-precursor in applications where the hydrophobicity is crucial.

Acknowledgments The authors gratefully acknowledge Pedro Nuno Simões for the experimental support in the thermal analysis experiments.

Appendix

Characteristic vibrations frequencies of FTIR spectra of the synthesized materials and the ascribed structural units are shown in Table 6. The presented values correspond to the minima of the observed peaks.

References

- Pierre AC, Pajonk GM (2002) Chemistry of aerogels and their applications. *Chem Rev* 102:4243–4265
- Dorcheh AS, Abbasi MH (2008) Silica aerogels; synthesis, properties and characterization. *J Mater Process Technol* 199:10–26
- Durães L, Nogueira S, Santos A, Preciso C, Hernandez J, Portugal A (1999) Flexible silica based xerogels and aerogels for spatial applications In: Ferreira, E., Mota, M. (Eds.), Proc. of the 10th International Chemical and Biological Engineering Conference—CHEMPOR 2008, Department of Biological Engineering of University of Minho, Braga, 2008, p 563
- Durães L, Ochoa M, Portugal A, Duarte N, Dias J, Rocha N, Hernandez J (2010) Tailored silica based xerogels and aerogels for insulation in space environments. *Adv Sci Technol* 63:41–46
- Durães L, Ochoa M, Rocha N, Patrício R, Duarte N, Redondo V, Portugal A (2011) Effect of the drying conditions on the microstructure of silica based xerogels and aerogels. *J Nanosci Nanotechnol* (accepted)
- Bhagat SD, Oh C-S, Kim Y-H, Ahn Y-S, Yeo J-G (2007) Methyltrimethoxysilane based monolithic silica aerogels via ambient pressure drying. *Microporous Mesoporous Mater* 100:350–355
- Rao AV, Kulkarni MM, Amalnerkar DP, Seth T (2003) Superhydrophobic silica aerogels based on methyltrimethoxysilane precursor. *J Non-Cryst Solids* 330:187–195
- Rao AV, Bhagat SD, Hirashima H, Pajonk GM (2006) Synthesis of silica aerogels using methyltrimethoxysilane (MTMS) precursor. *J Colloid Interface Sci* 300:279–285
- Tang Q, Xim B, Lee M (1999) Monolithic columns containing sol-gel bonded octodecylsilica for capillary electrochromatography. *J Chromatogr A* 873:35–50
- Loy D, Baugher B, Baugher C, Schneider D, Rahimain K (2000) Substituent effects on the sol-gel chemistry of organotrialkoxysilanes. *Chem Mater* 12:3624–3632
- Harrel J, Ebina T, Tsubo N, Stucky G (2002) Manipulation of pore size distributions in silica and ormosil gels dried under ambient pressure conditions. *J Non-Cryst Solids* 298:241–251
- Sumuneva B, Djambaski P, Kashchieva E, Chernev G, Kabaiyanova L, Emanuilova E, Salvado I, Fernandes M, Wu A (2008) Sol-gel synthesis and structure of silica hybrid biomaterials. *J Non-Cryst Solids* 354:733–740
- Al-Oweini R, El-Rassy H (2009) Synthesis and characterization by FTIR spectroscopy of silica aerogels prepared using several $\text{Si}(\text{OR})_4$ and $\text{R}''\text{Si}(\text{OR}')_3$. *J Mol Struct* 919:140–145
- Anderson A, Carroll M, Green E, Melville J, Bono M (2010) Hydrophobic silica aerogels prepared via rapid supercritical extraction. *J Sol-Gel Sci Technol* 53:199–207
- Lana S, Seddon A (1998) X-Ray diffraction studies of sol-gel derived ORMOSILs based on combinations of tetramethoxysilane and trimethoxysilane. *J Sol-Gel Sci Technol* 13:461–466
- Orel B, Jese R, Vilcnik A, Stangar U (2005) Hydrolysis and solvolysis of methyltriethoxysilane catalyzed with HCl or trifluoroacetic acid: IR spectroscopic and surface energy studies. *J Sol-Gel Sci Technol* 34:251–265